Neurobiology of Disease

The Polycomb Group Gene *Bmi1* Regulates Antioxidant Defenses in Neurons by Repressing *p53* Pro-Oxidant Activity

Wassim Chatoo,[1]* Mohamed Abdouh,[1]* Jocelyn David,[1] Marie-Pier Champagne,[1] José Ferreira,[2] Francis Rodier,[4] and Gilbert Bernier[1,3]

[1]Developmental Biology Laboratory and [2]Department of Pathology, Maisonneuve-Rosemont Hospital, Montreal, Quebec, Canada H1T 2M4, [3]Department of Ophthalmology, University of Montreal, Montreal, Quebec, Canada H3T 1J4, and [4]Lawrence Berkeley National Laboratory, Berkeley, California 94720

Aging may be determined by a genetic program and/or by the accumulation rate of molecular damages. Reactive oxygen species (ROS) generated by the mitochondrial metabolism have been postulated to be the central source of molecular damages and imbalance between levels of intracellular ROS and antioxidant defenses is a characteristic of the aging brain. How aging modifies free radicals concentrations and increases the risk to develop most neurodegenerative diseases is poorly understood, however. Here we show that the Polycomb group and oncogene Bmi1 is required in neurons to suppress apoptosis and the induction of a premature aging-like program characterized by reduced antioxidant defenses. Before weaning, *Bmi1*$^{-/-}$ mice display a progeroid-like ocular and brain phenotype, while *Bmi1*$^{+/-}$ mice, although apparently normal, have reduced lifespan. Bmi1 deficiency in neurons results in increased p19^{Arf}/p53 levels, abnormally high ROS concentrations, and hypersensitivity to neurotoxic agents. Most *Bmi1* functions on neurons' oxidative metabolism are genetically linked to repression of *p53* pro-oxidant activity, which also operates in physiological conditions. In *Bmi1*$^{-/-}$ neurons, p53 and corepressors accumulate at antioxidant gene promoters, correlating with a repressed chromatin state and antioxidant gene downregulation. These findings provide a molecular mechanism explaining how *Bmi1* regulates free radical concentrations and reveal the biological impact of *Bmi1* deficiency on neuronal survival and aging.

Key words: **Bmi1; p53; neuronal cell death; ROS; antioxidant; aging**

Introduction

Mitochondria are required for cellular aerobic respiration but are also the main source of intracellular reactive oxygen species (ROS), which are thought to be causal for most oxidative damage that accumulates with age (Balaban et al., 2005; Halliwell, 2006; Lin and Beal, 2006). The balance between ROS and antioxidant molecules is critical to determine the rate of oxidative damage accumulation, and thus possibly cellular and organism lifespan (Harman, 1956).

The role of the p53 gene in organism aging and on cellular oxidative metabolism remains highly controversial. A constitutively active form of p53 was shown to induce a premature aging-like phenotype in mice, while expression of a dominant-negative form of p53 in the CNS of *Drosophila* was shown to result in lifespan extension, both suggesting that *p53* activity promotes aging (Tyner et al., 2002; Bauer et al., 2005). In cell lines, p53 overexpression can also repress glutathione *S*-transferase α1 (GSTα1), NAD(P)H quinone oxidoreductase (NQO1), and cystine/glutamate transporter (xCT) expression, and interfere with antioxidant defenses activated by Nrf2 (Faraonio et al., 2006). In contrast, transgenic mice expressing an extra dose of the *p53* and *p19^{Arf}* genes have reduced tumor incidence and extended median but not maximum lifespan, and show increased resistance to paraquat (Matheu et al., 2007). P53 is proposed to mediate these biological effects by reducing ROS through activation of Sestrin1 and Sestrin2 (Sablina et al., 2005; Matheu et al., 2007). Whether p53 is a proaging or antiaging gene and whether its activity is pro-oxidant or antioxidant thus remains an open question.

Bmi1 is a member of the Polycomb group family. Polycomb group proteins form large multimeric complexes that silence specific target genes by modifying chromatin organization (Valk-Lingbeek et al., 2004). *Bmi1*$^{-/-}$ mice show axial skeleton defects and impaired development and degeneration of the cerebellum (Jacobs et al., 1999). *Bmi1* is required for the proliferation of hematopoietic and neural stem cells (Lessard and Sauvageau, 2003; Molofsky et al., 2003; Park et al., 2003). *Bmi1*-deficient stem cells and mouse embryonic fibroblasts (MEFs) proliferate poorly owing to derepression of the *Ink4a/Arf* locus (Jacobs et al., 1999; Molofsky et al., 2003). The *Ink4a/Arf* locus encodes two tumor suppressor proteins: p16^{Ink4a} and p19^{Arf}. P16^{Ink4a} is a cyclin-dependent kinase inhibitor that blocks the activity of Cdk4/6 by preventing its association with cyclin D, which results

Received Nov. 4, 2008; accepted Dec. 2, 2008.

This work was supported by grants from the Canadian Institutes of Health Research, Natural Science and Engineering Research Council of Canada, and Turmel Family Foundation for Macular Degeneration Research. F.R. was supported by National Institutes of Health Program Project Grant AG017242 to Judith Campisi. G.B. is supported by the Fonds de Recherche en Santé du Québec. W.C. is a Scholar from the Fonds de Recherche en Ophtalmologie de l'Université de Montréal. We thank M. van Lohuizen for Bmi1$^{+/-}$ mice, G. Ferbeyre for the DNp53 virus, and E. Drobetsky, E. Milot, and L. Levin for critical reading of this manuscript.

*W.C. and M.A. contributed equally to this work.

Correspondence should be addressed to Gilbert Bernier, Developmental Biology Laboratory, Maisonneuve-Rosemont Hospital, 5415 Boulevard de l'Assomption, Montreal, Quebec, Canada H1T 2M4. E-mail: gbernier.hmr@ssss.gouv.qc.ca.

DOI:10.1523/JNEUROSCI.5303-08.2009

 0270-6474/09/290529-14$15.00/0

in Rb hypophosphorylation and cell cycle arrest or senescence. $P19^{Arf}$ binds and inhibits the activity of the E3-ubiquitin ligase mouse double minute 2 (Mdm2), which prevents p53 targeting for proteasomal degradation (Sherr, 2001; Sharpless et al., 2004).

We show here that Bmi1 is expressed in ocular tissues and in postmitotic neurons of the CNS. *Bmi1*$^{-/-}$ mice display a progeroid-like ocular and brain phenotype, while *Bmi1*$^{+/-}$ mice have reduced lifespan. *Bmi1*$^{-/-}$ neurons are hypersensitive to several neurotoxic agents. They also present abnormally high ROS concentrations, increased $p19^{Arf}$/p53 levels, and dramatic reduction in antioxidant defenses. Genetic and molecular analyses revealed that most *Bmi1* effects on neurons' oxidative metabolism are linked to repression of *p53* pro-oxidant activity, which also operates in physiological conditions.

Materials and Methods

Mice. Bmi1$^{-/-}$ mice (in the C57BL/6 background) are a gift from M. van Lohuizen (The Netherlands Cancer Institute, Amsterdam, The Netherlands). *p53* heterozygote mice (B6.129S2-Trp53tm1Tyj/J) were purchased from The Jackson Laboratory. Wild-type (WT) C57BL/6 inbred mice (Charles River) were maintained in our facilities and used in accordance with the Animal Care Committee of the Maisonneuve-Rosemont Hospital Research Centre.

Neuronal cultures. Embryonic day 18.5 cortical neuron cultures were established by mechanical dissociation of the cortices into a single-cell suspension. Cells were plated at 1.5×10^5 cells/well on poly-L-lysine-coated eight-well cultures slides (BD Biosciences) in serum-free media containing Neurobasal-A medium (Invitrogen), Glutamax-I (Invitrogen), gentamycin (50 μg/ml; Invitrogen), B27 supplement (Invitrogen), NGF (50 ng/ml; Invitrogen), and BDNF (0.5 ng/ml; Invitrogen). For the β-amyloid transfection experiments, the human β-amyloid (1–42 form) (from n1953 to n2081; GenBank accession no. NM_201413) cDNA was cloned by RT-PCR using human retina, and inserted into the DUAL-IRESGFP plasmid. The plasmid was purified on cesium chloride column by ultracentrifugation. Neurons were nucleofected with plasmid DNA using the Mouse Neuron Nucleofector Kit according to manufacturer's instructions (Amaxa Biosystems). In these experiments, electroporation efficiency was ~10%.

Mouse embryonic fibroblasts. Cultures were established from day 14 (MEFs) or day 18 (MELFs) embryos and cultured at 3% or 20% oxygen concentration in DMEM containing 10% FBS and gentamycin (50 μg/ml; Invitrogen). Cells were frozen after the first passage following establishment and were considered at population doubling zero (PD 0) at this point. Cell number was determined and population doubling calculated at each passage. MEFs (PD 0) were infected overnight with high-titer lentiviruses encoding either GFP or GSE22, a genetic suppressor element of p53 [for details on lentivectors used, see Beauséjour et al. (2003)]. Lentiviral titers were adjusted to infect >90% of cells, and infection rates were verified by immunohistochemistry.

Immunolabeling. For fixation, tissues were immersed for 1 h at room temperature in 4% paraformaldehyde (PFA)/3% sucrose in 0.1 M phosphate buffer, pH 7.4. Samples were washed three times in PBS, cryoprotected in PBS/30% sucrose, and frozen in CRYOMATRIX embedding medium (CEM) (Thermo Shandon). Otherwise, tissues were fixed in 10% buffered formalin and embedded in paraffin according to standard protocols. Five- to seven-micrometer-thick sections were mounted on Super-Frost glass slides (Fisher Scientific) and processed for immunofluorescence or immunohistochemistry staining. For immunofluorescence labeling, sections were incubated overnight with primary antibody solutions at 4°C in a humidified chamber. After three washes in PBS, sections were incubated with secondary antibodies for 1 h at room temperature. Slides were mounted on coverslips in DAPI-containing mounting medium (Vector Laboratories). For immunohistochemistry labeling, formalin-fixed paraffin-embedded slices were analyzed by using the Vectastain ABC kit (Vector) according to the manufacturer instructions. Peroxidase substrates used are the Vector VIP (pink) (Vector), and DAB (brown) (Sigma). Observations were made under a fluorescence microscope (Leica DMRE, Leica Microsystems) and images were captured with a digital camera (Retiga EX; QIMAGING; with OpenLab, version 3.1.1 software). Antibodies used in this study were sheep anti-Chx10 (Exalpha Biologicals); rabbit anti-Pax6, rabbit anti-MAP2, mouse anti-NeuN, and rabbit anti-GFAP (DAKO); rabbit anti-cleaved caspase-3 (Cell Signaling); mouse anti-mouse Bmi1, mouse anti-human Bmi1, and rabbit anti-human Bmi1 (US Biological); rabbit anti-$p19^{Arf}$ (Abcam); and mouse anti-BrdU (Sigma). Secondary antibodies used were FITC-conjugated donkey anti-mouse and rhodamine-conjugated donkey anti-rabbit (Millipore Bioscience Research Reagents) and AlexaFluor633-conjugated donkey anti-sheep (Invitrogen).

Real-time RT-PCR. All primers were designed to flank individual exons and tested by PCR in RT^+ and RT^- control extracts. Total RNA was isolated using TRIzol reagent (Invitrogen). Reverse transcription (RT) was performed using 1 μg of total RNA and the MML-V reverse transcriptase (Invitrogen). PCR amplification was performed using the HotStar TAQ polymerase (Invitrogen). PCR was run as follows: 94°C for 10 min, followed by 30 cycles of denaturing at 94°C, annealing at 57°C, and extension at 72°C in an Applied Biosystems thermal cycler. Real-time PCR was performed using the Platinum SYBRGreen SuperMix (Invitrogen) and a real-time PCR apparatus (Bio-Rad). Primers sets used were as follows: Bmi1 (F) 5′-GGAGACCAGCAAGTATTGTCCTATTTG-3′; (R) 5′-CTTACGATGCCCAGCAGCAATG-3′, $p16^{Ink4a}$ (F) 5′-CAACGCCCCGAACTCTTTC-3′; (R) 5′-GCAGAAGAGCTGCTACGTGAAC-3′, $p19^{Arf}$ (F) 5′-GGCTAGAGAGGATCTTGAGAAGAGG-3′; (R) 5′-GCCCATCATCATCACCTGGTCCAGG-3′, bcl2l2 (F) 5′-GACGAGTTTGAGACCCGTTT-3′; (R) 5′-ATCCAATCCTGCACTTGTCC-3′, Noxa (F) 5′-AGTTCGCAGCTCAACTCAGG-3′; (R) 5′-GCCGTAAATTCACTTTGTCTCC-3′, Puma (F) 5′-CAAGAAGAGCAGCATCGACA-3′; (R) 5′-TAGTTGGGCTCCATTTCTGG-3′, Apaf1 (F) 5′-TGCTCAGCGGATAAGAAGGT-3′; (R) 5′-TCCCAGAGCTTGAGGAAGAA-3′, xCT (F) 5′-TGGAGGTCTTTGGTCCTTTG-3′; (R) 5′-CCAGGATGTAGCGTCCAAAT-3′, GST-1α (F) 5′-CGCCACCAAATATGACCTCT-3′; (R) 5′-CCATGGCTCTTCAACACCTT-3′, NQO1 (F) 5′-TTCTCTGGCCGATTCAGAGT-3′; (R) 5′-GAGTGTGGCCAATGCTGTAA-3′, Sod1 (F) 5′-CGGATGAAGAGAGGCATGTT-3′; (R) 5′-CACCTTTGCCCAAGTCATCT-3′, Sod2 (F) 5′-GGCCAAGGGAGATGTTACAA-3′; (R) 5′-GCTTGATAGCCTCCAGCAAC-3′, Sestrin1 (F) 5′-TCGTGTGCACTCCTGAAAAG-3′; (R) 5′-TACCGGGTAATGGCTCTCAG-3′, Sestrin2 (F) 5′-CCTCCTTTGTGTTGTGCTGT-3′; (R) 5′-ACGGTTCTCCATTTCCTCCT-3′, and hprt (F) 5′-ACTGTAATGATCAGTCAACGGG-3′; (R) 5′-GGCCTGTATCCAACACTTGG-3′.

Western blotting. WT and *Bmi1*$^{-/-}$ neurons were homogenized in lysis buffer (10 mM Tris, 10 mM NaCl, 3 mM $MgCl_2$, 0.5% NP-40, and protease inhibitor cocktail). Following centrifugation at 10,000 rpm at 4°C for 10 min, pellets containing nuclei were dissolved in resuspension buffer (10 mM HEPES, 0.4 mM NaCl, 1.5 mM $MgCl_2$, 1 mM EDTA, 1 mM DTT, and protease inhibitors). Samples were ultracentrifuged at 55,000 rpm at 4°C for 10 min, and supernatants containing nuclear extracts were analyzed by immunoprecipitation. Otherwise, total protein extracts were prepared in buffer K (20 mM sodium phosphate, pH 7.0, 150 mM KCl, 30 mM sodium pyrophosphate, 0.1% NP-40, 5 mM EDTA, 10 mM NaF, 0.1 mM Na_3VO_4, and protease inhibitors). Proteins contents were quantified using the Bradford reagent. For immunoprecipitation, we used a sheep anti-p53 polyclonal antibody (EMD Biosciences), and Salmon Sperm DNA-protein A/G beads (Millipore). Beads with bound immunocomplexes were washed with buffer K, and bound proteins were heat eluted with Laemmli buffer. Eluted proteins were resolved by SDS-PAG electrophoresis and transferred to a nitrocellulose blotting membrane (Pall) that was exposed to an anti-acetylated lysine antibody (Cell Signaling). For Western blots on total protein extracts, the primary antibodies used were rabbit anti-p53 polyclonal antibody, anti-Nrf2 polyclonal antibody, and anti-PGC-1α polyclonal antibody (Santa Cruz Biotechnology), anti-Sirt1 polyclonal antibody, anti-phospho-histone H2A.X monoclonal antibody (Millipore), and anti-β-actin monoclonal antibody (Abcam). Membranes were treated with corresponding horseradish peroxidase-conjugated secondary antibodies (Sigma) and developed using the Immobilon Western (Millipore).

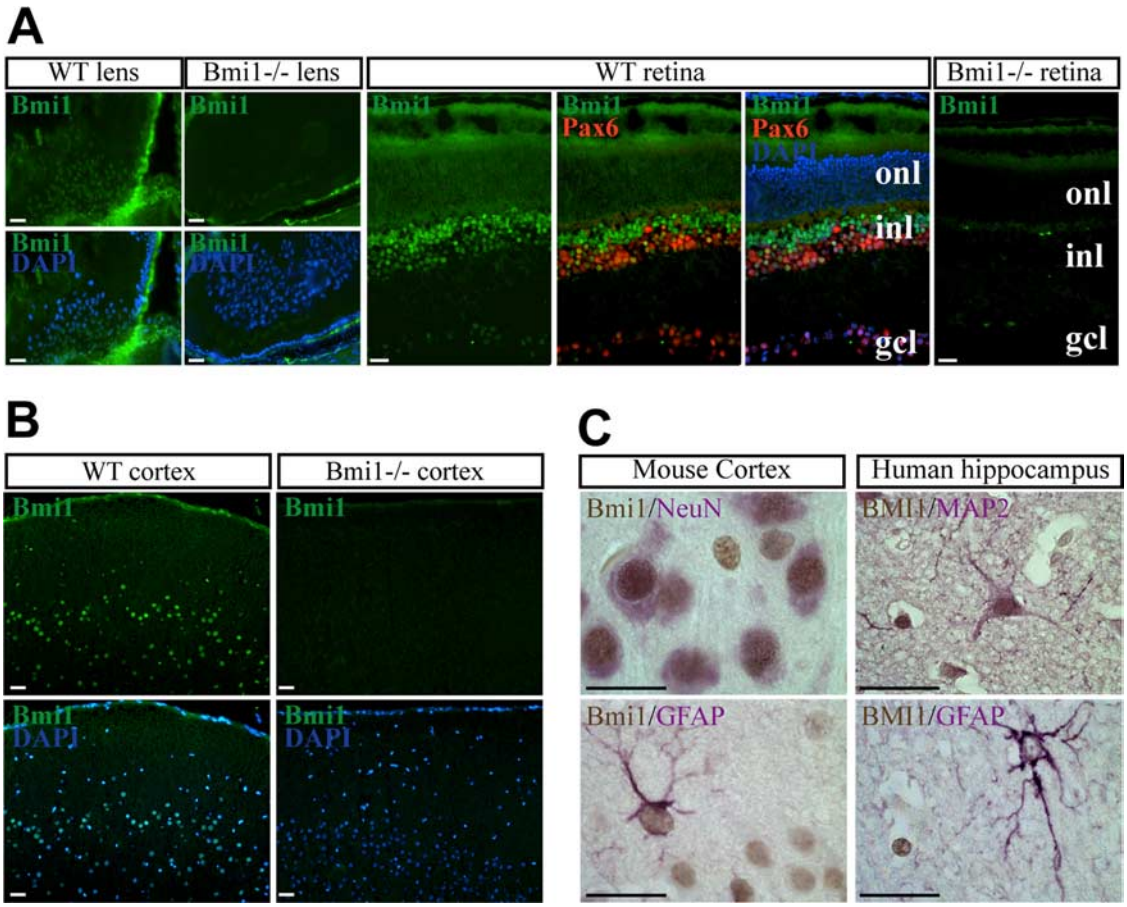

Figure 1. Bmi1 is expressed in postmitotic neurons of the CNS. ***A***, Frozen eye sections from d25 WT and *Bmi1* $^{-/-}$ littermates were analyzed by immunofluorescence. No specific Bmi1 labeling was detected in *Bmi1* $^{-/-}$ samples. ***B***, Brain sections from d25 WT and *Bmi1* $^{-/-}$ littermates were analyzed as in ***A***. ***C***, Mouse and human brain sections were analyzed by immunohistochemistry (Bmi1 is in brown; MAP2, NeuN, and GFAP are in pink). Scale bars, 20 μm. onl, Outer nuclear layer; inl, inner nuclear layer; gcl, ganglion cell layer.

Chromatin immunoprecipitation. Chromatin immunoprecipitation (ChIP) was performed using the ChIP Assay kit (Millipore). Briefly, 1–1.5 $\times$ 10^6 fixed cells were sonicated to shear the chromatin and immunoprecipitated using mouse anti-p53 (DO-1), goat anti-N-CoR (Santa Cruz), rabbit anti-H3Me2Lys9, rabbit anti-H3Me2Lys27 (Cell Signaling), rabbit anti-HDAC1, rabbit anti-acetyl-H4, and anti-mouse IgG (Millipore) antibodies. Promoter fragments were amplified using primers to x-CT, Sod2, and β-major chain as follows: x-CT (−193 to +15); (F) 5′-ATCCATTGAGCAACCCACA-3′ and (R) 5′-AGCTGAGCTGGTGTGTAATG-3′, and Sod2 (−537 to +23); (F1) 5′-CAAACCTGCGACGTGATTTA-3′, (R1) 5′-AGCTGCAAAGCTTCCACTCT-3′, (F2) 5′-AATTTGGCACAGGGGAGAC-3′ and (R2) 5′-CGCCCGACACAACATTATT-3′ for site 1 and site 2, respectively, and β-major (F) 5′-CAGTGAGTGGCACAGCATCC-3′, (R) 5′-CAGTCAGGTGCACCATGATGT-3′.

Microarray analyses. Total RNA was prepared using TRIzol reagent (Invitrogen) and purified by the RNeasy MiniElute Cleanup kit (Qiagen) from 5 WT and 5 *Bmi1* $^{-/-}$ neuronal cultures. Microarray analysis using BeadChip Mouse Genome (Illumina) was performed at the Centre d'innovation at Genome Quebec (McGill University, Montreal, Quebec, Canada). Data were analyzed using the FlexArray software.

Senescence-associated β-galactosidase assay. Senescence-associated (SA) β-galactosidase staining was detected histochemically at pH 6 as described previously (Dimri et al., 1995). Briefly, tissue slices were fixed in PBS containing 1% formaldehyde, 0.4% glutaraldehyde, and 0.02% Igepal. After three washes, slices were exposed to the X-gal solution (1 mg/ml X-gal; 5 mM $K_3Fe(CN)_6$; 5 mM $K_4Fe(CN)_6$; 1 mM $MgCl_2$, in PBS; pH 6.0). Slides were mounted and observations made under a microscope (Leica DMRE, Leica Microsystems), and images were captured with a digital camera (Retiga EX; QIMAGING; with OpenLab, version 3.1.1 software).

Cell viability analysis. For apoptosis, activated caspase-3 staining was performed by IHC using a rabbit anti-cleaved caspase-3 antibody (Cell Signaling). For the quantification of caspase-3-independent cell death (i.e., vacuolization), neurons' overall morphology was visualized by IHC using the rabbit anti-MAP2 (Cell Signaling). Grades of vacuolization were determined empirically according the vacuole density inside the cell. The measure is qualitative by nature (grade I, few small vacuoles, i.e., close to but not normal; grade II, more vacuoles: clearly abnormal; grade III, filled with vacuoles: near autolysis).

ROS and lipid peroxidation levels. Cortices were prepared on ice before homogenization while cultured embryonic neurons were collected following trypsin treatment (TrypLE Express, Invitrogen). Samples were homogenized in a Potter-Elvehjem homogenizer in 5 mM Tris-HCl buffer, pH 7.4 (Merck). The dichlorodihydrofluorescein diacetate (DCF-DA; Sigma) staining method was used for the quantification of ROS generation (Radák et al., 2004). The dye was added to the homogenates to achieve a final concentration of 25 μM. Fluorescence intensity was monitored using a fluorescence multiwell plate reader (Perseptive Biosystems), at excitation 485 nm and emission 530 nm. On the other hand, homogenates were tested for lipid peroxidation by measuring the concentration of malondialdehyde (MDA) according to the thiobarbituric acid reactive substrate (TBARS) method (Buege and Aust, 1978). The homogenates were mixed to 0.6% TBA mixture and boiled for 30 min. After cooling on ice, the chromogenic reaction was read in a spectrophotometer (Beckman) at 535 nm. Data are normalized to the amounts of proteins per sample.

Statistical analysis. Statistical differences were analyzed using Student's

t test for unpaired samples. An ANOVA followed by the Dunnett test was used for multiple comparisons with one control group. For nonparametric data analysis (i.e., cataract incidence phenomenon), a χ^2 test was performed. The criterion for significance (p value) was set as mentioned in the figures.

Results

Bmi1 is expressed in ocular tissues and postmitotic neurons of the mature CNS

In the rodent eye, all retinal cells are postmitotic by postnatal day (d) 25, and we observed robust Bmi1 expression in retinal neurons, ciliary body epithelium (CBE), and lens cells of d25 and 9-month-old mice (Fig. 1*A*, data not shown). Dual immunofluorescence using antibodies against the lineage-specific markers Chx10 and Pax6 showed that in the retina, Bmi1 is expressed in bipolar and ganglion cells and a subset of amacrine cells. Bmi1 was also detected in mouse and human photoreceptors (Fig. 1*A*, data not shown). In the mouse brain, Bmi1 was expressed in cells of the upper cortical layers and the hippocampus, but not in the white matter (Fig. 1*B*, data not shown). Most CNS neurons in both humans and mice expressed Bmi1 (Fig. 1*B*,*C*), while only some astrocytes in mice did (Fig. 1*C*). These data indicate that Bmi1 is robustly expressed in ocular tissues and in nearly all postmitotic neurons of the developing and adult CNS of mice and men.

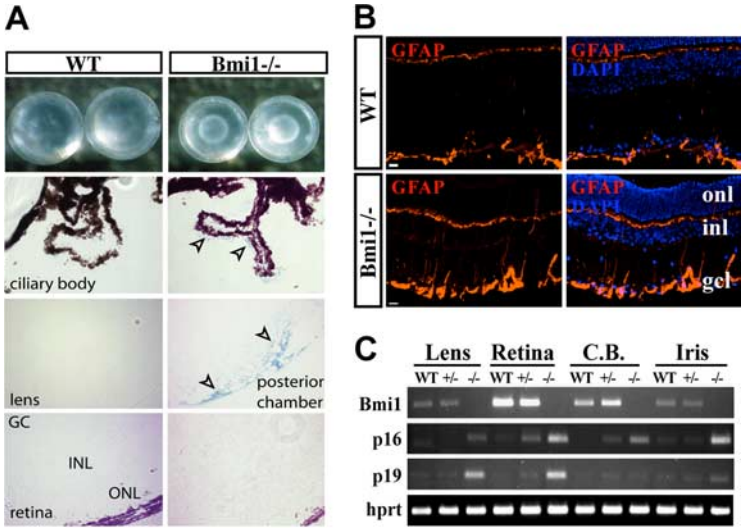

Figure 2. *Bmi1* deficiency results in an early aging-like phenotype in the eye. ***A***, Lenses from *Bmi1* $^{-/-}$ mice show visible cataracts (top panels). Frozen eye sections from WT and *Bmi1* $^{-/-}$ littermate mice were stained for SA β-galactosidase activity (arrowheads). ***B***, Immunofluorescence analysis of 3-week-old WT and *Bmi1* $^{-/-}$ mice retinal sections labeled with a GFAP antibody. GFAP (red) is overexpressed in *Bmi1* $^{-/-}$ retina. onl, Outer nuclear layer; inl, inner nuclear layer; gcl, ganglion cell layer; C.B., ciliary body. Scale bars, 20 μm. ***C***, Gene expression was analyzed by RT-PCR in WT, *Bmi* $^{+/-}$, and *Bmi1* $^{-/-}$ eye structures. *hprt* was used as internal standard.

Bmi1 deficiency results in a premature aging-like ocular phenotype

During the course of our study, we found that ~90% of *Bmi1* $^{-/-}$ mice ($n = 10$, $p = 0.001$) in the C57BL/6 genetic background presented bilateral lens cataracts at d20–d25 (Fig. 2*A*); remaining *Bmi1* $^{-/-}$ mice had unilateral cataracts ($n = 2$). No cataracts were found in WT littermates at this early age ($n = 10$). Lens cataracts are well established biomarker of aging (The Italian-American Cataract Study Group, 1991; Wolf et al., 2005). In cell dissociation assays, we also found that the CBE of *Bmi1* $^{-/-}$ mice was more sensitive to protease treatment than that of WT littermates, with ≥90% of cell viability for 8 min of protease treatment for WT ($n = 5$), and ≥90% of cell viability at 6 min 50 s of protease treatment for *Bmi1* $^{-/-}$ ($n = 3$, $p = 0.04$). This suggests that Bmi1 deficiency compromises the structural integrity of the CBE extracellular matrix. Alterations of the extracellular matrix are found in eyes of aged mammals (Ihanamäki et al., 2001). To evaluate whether the observed cataracts were due to a developmental defect or to accelerated aging, we tested the eyes for the presence of SA β-galactosidase activity, an enzymatic biomarker of cellular senescence (Dimri et al., 1995). We observed robust staining for the SA β-galactosidase activity in the lens, and weaker staining in the CBE of *Bmi1* $^{-/-}$ mice (Fig. 2*A*). Reactive gliosis in the retina and brain is observed in neurodegenerative diseases and CNS lesions and during normal aging in humans and mice (Silver and Miller, 2004). Likewise, *Bmi1* $^{-/-}$ mice had a reactive gliosis in the retina at d25 (Fig. 2*B*). Upregulation of p16 ^{Ink4a} and p19 ^{Arf} genes has been correlated with normal tissue aging *in vivo*, and we could confirm this in the CNS of aging mice and humans by analyzing protein and gene expression (data not shown) (Krishnamurthy et al., 2004). We dissected eye structures (lens, retina, iris, and CBE) from WT and *Bmi1* $^{-/-}$ littermates at d25, and evaluated p16 ^{Ink4a} and p19 ^{Arf} genes expression. Compared with WT mice, expression of both genes was increased in most eye structures of *Bmi1* $^{-/-}$ mice, including the retina (Fig. 2*C*). These findings reveal that *Bmi1* deficiency results in a premature aging-like ocular phenotype.

Bmi1 gene dosage modulates lifespan

Bmi1 $^{+/-}$ mice are fertile and apparently normal, in contrast with *Bmi1* $^{-/-}$ mice, which present growth defects and a lethality rate exceeding 75% before weaning (Jacobs et al., 1999). However, we noticed that ~10% of *Bmi1* $^{+/-}$ mice developed lens cataracts by the time of weaning, in contrast to their WT littermates, which did not have cataracts at this early age. This suggested the possibility that Bmi1 gene dosage may influence cellular aging and organism lifespan. To assess the potential involvement of Bmi1 gene dosage in the regulation of lifespan, we analyzed cohorts of WT and *Bmi1* $^{+/-}$ mice in the C57BL/6 genetic background over a period of 36 months. In general, *Bmi1* $^{+/-}$ mice were indistinguishable from their WT littermates. However, at 15 months of age they progressively presented features resembling those of 22- to 24-month-old C57BL/6 WT mice, such as hair loss covering >20% of body surface, lens cataracts, and reduced locomotor activity. Kaplan-Meyer analysis revealed that loss of one Bmi1 allele reduced the median and maximum lifespan by ~35% (Fig. 3*A*). These data reveal that Bmi1 gene dosage can modulate lifespan.

Loss of *Bmi1* results in activation of a p53-dependent apoptotic cascade in CNS neurons

Consistent with Bmi1 expression in most postmitotic cortical neurons, we found a significant upregulation of $p16^{Ink4a}$ (174.9 ± 33.7, $p = 0.004$), $p19^{Arf}$ (5.3 ± 0.7, $p = 0.002$), and $p21^{Cip1}$ (1.9 ± 0.2, $p = 0.006$) in the cerebral cortex of *Bmi1* $^{-/-}$ mice ($n = 3$) at P20 when compared with WT littermates ($n = 4$), as measured by quantitative RT-PCR. Immunostaining also revealed robust p19 ^{Arf} expression in individual cortical neurons (NeuN $^{+}$) of

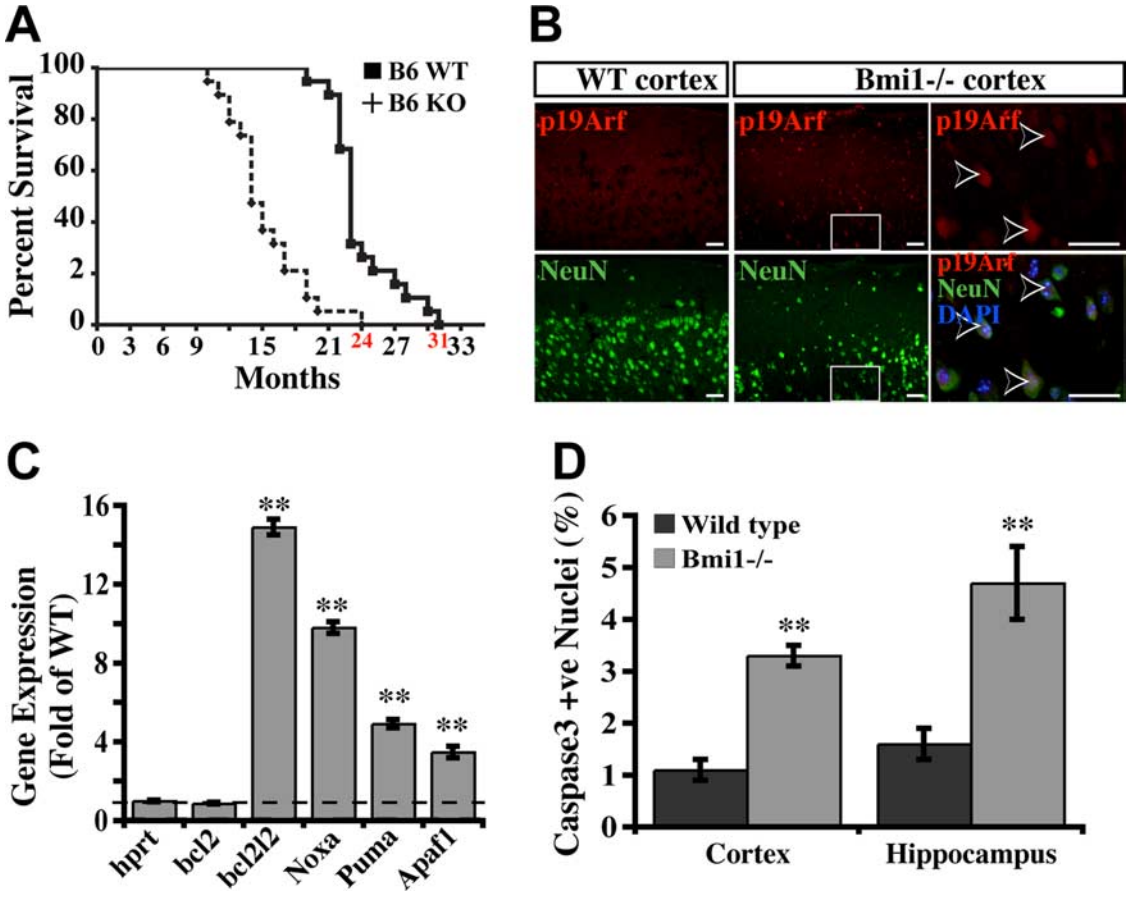

Figure 3. *Bmi1* modulates lifespan and neuronal apoptosis in the CNS. ***A***, Kaplan-Meyer representation of the survival curves of WT and $Bmi1^{+/-}$ mice (19 mice per cohort). Statistical significance was assessed using the log rank test relative to WT; $p < 0.0001$. ***B***, Cortical sections from d25 WT and $Bmi1^{-/-}$ littermates labeled with $p19^{Arf}$ and NeuN antibodies. Arrowheads indicate neurons expressing $p19^{Arf}$. Scale bars, 20 μm. ***C***, Real-time PCR analysis of genes expression in the $Bmi1^{-/-}$ cortex (relative to WT). Results are mean ± SD ($n = 4$ sets of brains; $^{**}p < 0.01$). ***D***, Immunohistochemistry analysis of WT and $Bmi1^{-/-}$ brain sections labeled with anti-caspase-3 antibodies. Data are expressed as the percentage of caspase-3^{+} nuclei over total hematoxylin-stained nuclei counts. Results are mean ± SD ($n = 5$; $^{**}p < 0.01$).

$Bmi1^{-/-}$ mice, but not of WT littermates (Fig. 3*B*). $P19^{Arf}$ increases p53 activity by inhibiting Mdm2-mediated p53 degradation (Sherr, 2006). The increased in $p19^{Arf}$ expression in retinal and cortical neurons of $Bmi1^{-/-}$ mice is thus predicted to increase p53 activity. One way p53 might promote aging in the CNS is by rending neurons more susceptible to apoptosis. Ectopic expression of p53 in mouse cortical neurons has been shown to induce apoptosis, and $p53^{-/-}$ neurons are resistant to apoptosis induced by the topoisomerase I inhibitor and DNA-damaging agent camptothecin (Fortin et al., 2001; Cregan et al., 2004). We quantified the expression of p53 target genes involved in apoptosis in the cortex of $Bmi1^{-/-}$ mice. Puma, Noxa, Bcl2l2, and Apaf1 expression were significantly increased (Fig. 3*C*). Furthermore, immunostaining for activated caspase-3, a marker of apoptosis, showed that, compared with WT, $Bmi1^{-/-}$ mice had a threefold to fivefold increased apoptosis in the cortex and hippocampus (Fig. 3*D*).

To evaluate p53 expression in the CNS of WT and *Bmi1*-null mice, we performed Western blot analysis on cortical extracts using antibodies against p53. In these conditions, p53 was not detectable. We rationalized that this could be explained by a dilution effect. To test this, we first analyzed Bmi1 expression in the embryonic cortex at e18.5, and found robust expression in cortical neurons (Fig. 4*A*). We then performed embryonic cortical neuron cultures from e18.5 WT and *Bmi1*-null littermates, where >95% of cells present after 7 d were postmitotic neurons expressing the neuronal marker MAP2 along with Bmi1 (Fig. 4*B*). As expected, $p16^{Ink4a}$ and $p19^{Arf}$ expression levels were increased in cultured $Bmi1^{-/-}$ neurons (Fig. 4*C*). We measured total p53 levels by Western blot at day 7 of culture. We found that in $Bmi1^{-/-}$ neurons, the total amount of p53 was increased near 3.5 times at normal oxygen tension (data not shown). To further validate our findings, we cultured WT and $Bmi1^{-/-}$ neurons at 3% oxygen concentration, to reduce oxidative stress. Using these conditions, we observed that total p53 was increased ~1.8 times in $Bmi1^{-/-}$ neurons compared with WT (Fig. 4*D*). One post-translational modification linked to p53 activation is lysine acetylation, and recent work revealed that p53 acetylation (but not phosphorylation) is indispensable for its growth arrest and apoptotic activities (Vaziri et al., 2001; Tang et al., 2008). We found that the acetylated form of p53 was increased ~2.2 times in $Bmi1^{-/-}$ neurons at normal oxygen tension (Fig. 4*D*). Because *Bmi1* deficiency may induce p53 activation through a $p19^{Arf}$-independent pathway, such as through increased DNA damage, we measured γH2AX levels by Western blot and immunofluorescence. γH2AX is a DNA damage sensor that also helps to maintain genome integrity, and DNA damage is followed by the accumulation of γH2AX foci in the cell nucleus. In both WT and $Bmi1^{-/-}$ neurons, γH2AX expression was not detected by Western blot, and no differences could be observed either by immunofluorescence (Fig. 4*E*, data not shown). Together, these results suggest that loss of *Bmi1* results in activation of a p53-dependent

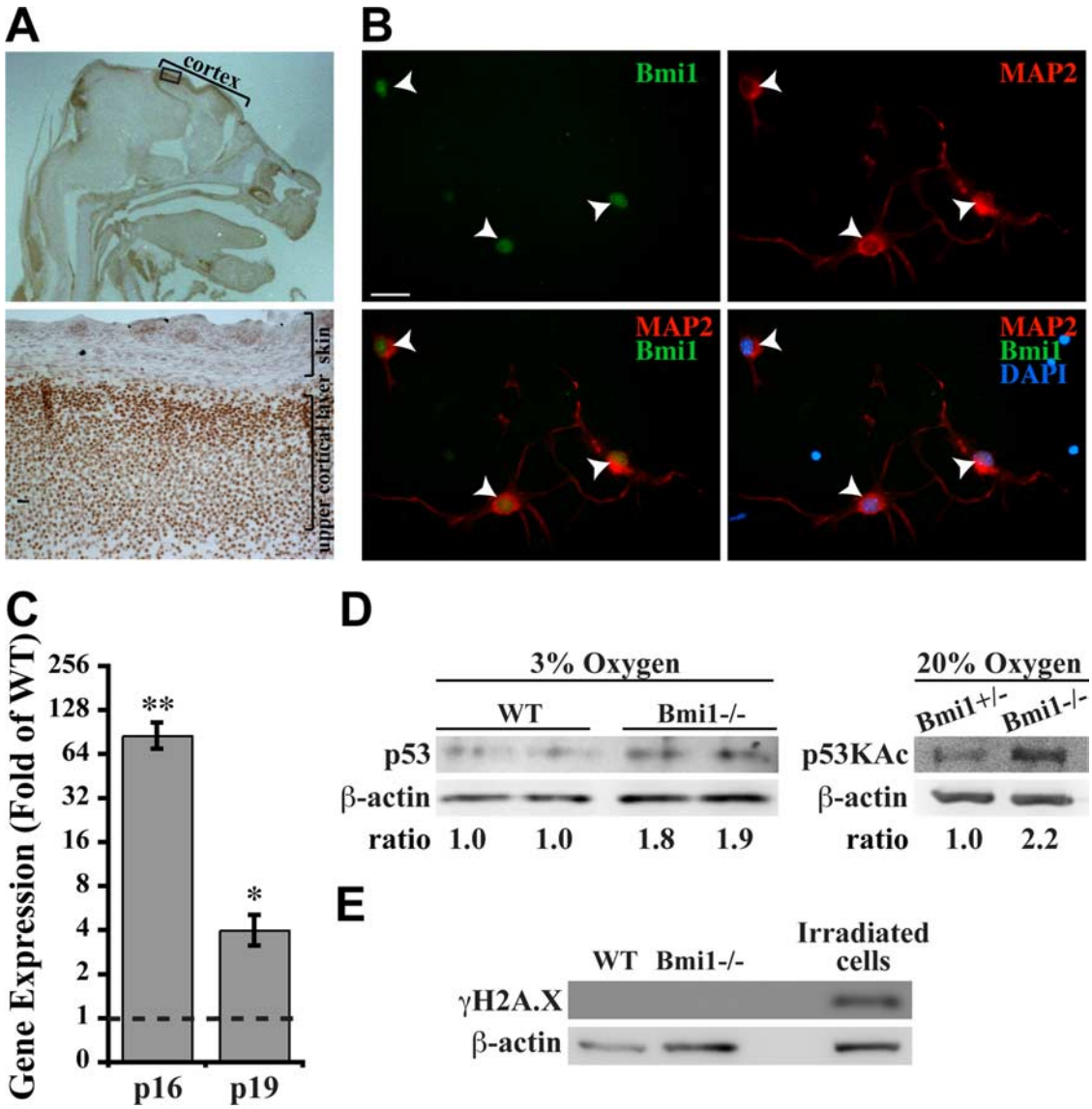

Figure 4. P53 expression level and activation state are enhanced in *Bmi1* $^{-/-}$ neurons. ***A***, ***B***, Bmi1 is expressed in embryonic cortical neurons. ***A***, Sections of mouse embryos (e18.5) were analyzed by IHC using a Bmi1 antibody. Bmi1 is highly expressed in neurons of the upper cortical layer. ***B***, Embryonic (e.18.5) neurons were cultured on poly-L-lysine substrate in serum-free media containing NGF and BDNF. Seven days later, they were labeled with Bmi1 and MAP2 antibodies and analyzed by immunofluorescence. Bmi1 (green) is coexpressed with the neuronal marker MAP2 (red) (arrowheads). Scale bars, 20 μm. ***C***, Real-time PCR analysis shows that $p16^{Ink4a}$ and $p19^{Arf}$ expression levels are increased in cultured *Bmi1* $^{-/-}$ neurons. Results are mean ± SD compared with WT levels set at 1 ($n = 3$–4 independent cell cultures; $^{*}p < 0.05$, $^{**}p < 0.01$). ***D***, Western blot analysis shows that the expression levels of total and acetylated p53 are increased in cultured *Bmi1* $^{-/-}$ neurons. Data are calculated as ratios of p53 levels to those of β-actin. Ratios in *Bmi1* $^{-/-}$ samples are compared with the ratios in WT samples set at 1 ($n = 3$ independent cultures; $p = 0.02$ for p53 expression analysis, and $p = 0.001$ for acetylated p53 expression analysis). ***E***, Western blot analysis of cultured WT and *Bmi1* $^{-/-}$ neurons using an anti-γH2AX antibody shows that γH2AX is not detected under these conditions. WT neural stem cells irradiated at 10 Gy were used as positive control.

apoptotic cascade in the cerebral cortex, and reveal that $p19^{Arf}$ expression as well as total p53 level and p53 activation state are increased in cultured *Bmi1* $^{-/-}$ neurons.

P53 inhibition can rescue *Bmi1* $^{-/-}$ MEFs senescence and proliferation phenotypes

Previous work revealed that *Bmi1* $^{-/-}$ MEFs proliferate poorly and become prematurely senescent at passage 3 (Jacobs et al., 1999). To evaluate the specific contribution of p53 to the phenotype of *Bmi1* $^{-/-}$ cells, we inhibited its activity in *Bmi1* $^{-/-}$ MEFs using a retrovirus expressing a dominant-negative form of p53 (GSE22). In mice, ambient oxygen (20%) concentration is sufficient to induce MEFs senescence through accumulation of oxidative damage and induction of p53 (Parrinello et al., 2003). To test the possibility that oxygen concentration may also influence the *Bmi1* $^{-/-}$ phenotype, we cultured MEFs at 3% and 20% oxygen concentration (Fig. 5*A–D*). We found that inactivation of p53 in *Bmi1* $^{-/-}$ MEFs lead to a gradual but almost complete rescue of growth capabilities in either 3% or 20% oxygen tension, revealing that p53 inactivation alone is sufficient to rescue both premature senescence and proliferation defects caused by the loss of *Bmi1* in MEFs.

Bmi1 $^{-/-}$ neurons are hypersensitive to neurotoxic agents in a p53-dependent manner

To address whether the apoptotic features observed in the CNS of *Bmi1* $^{-/-}$ mice were cell autonomous to neurons and p53 dependent, we used neuronal cultures. Neurons from both genotypes

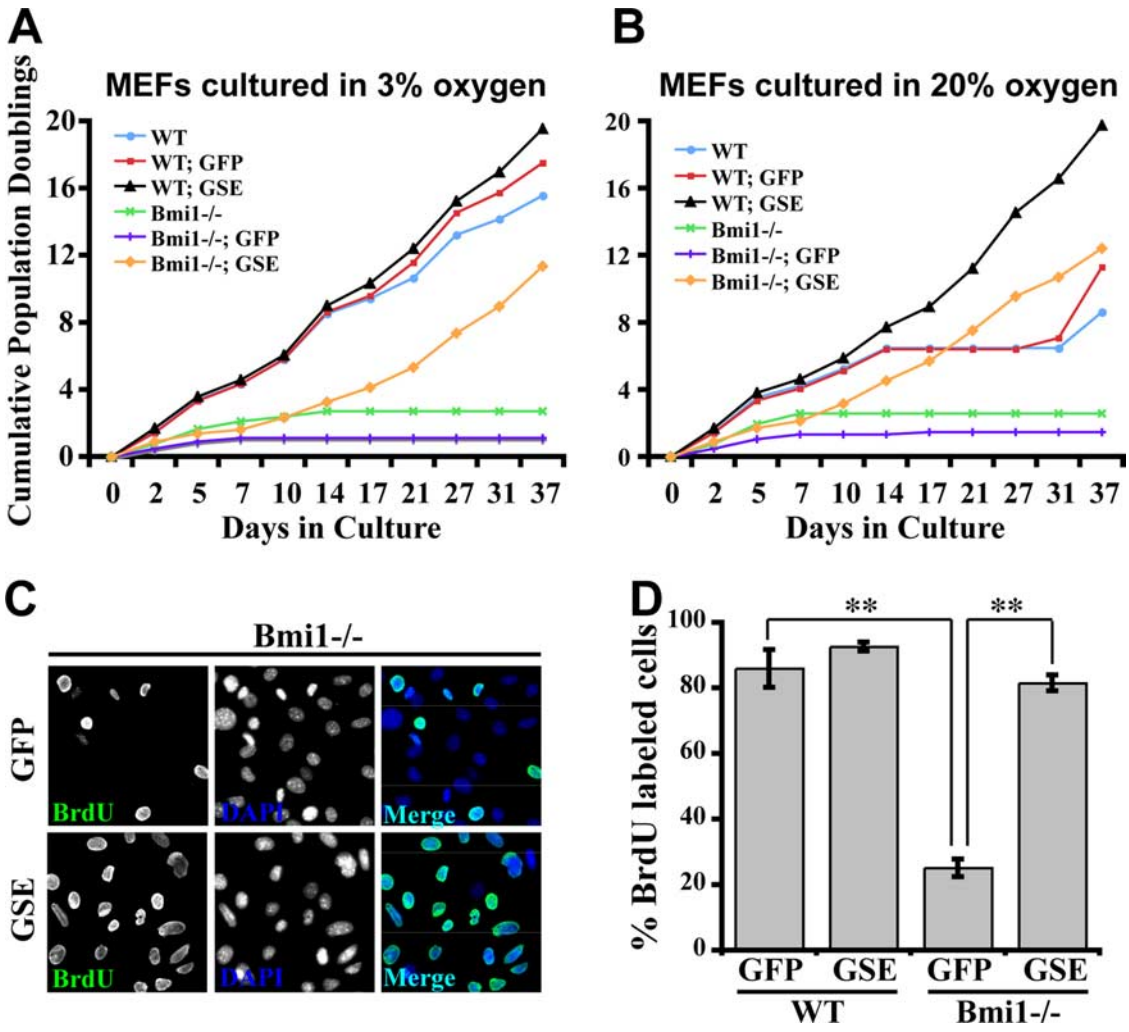

Figure 5. Premature senescence and slow proliferation phenotypes of *Bmi1* $^{-/-}$ MEFs are p53 dependent. ***A***, ***B***, WT and *Bmi1* $^{-/-}$ MEFs were cultured under 3% or 20% oxygen concentration and population doublings (PD) were calculated at every passage. Cells were infected at PD 0 with a control retrovirus encoding GFP (-GFP) or GSE-22 (-GSE), a dominant negative peptide that inactivates p53. GSE can rescue the premature senescence phenotype of *Bmi1* $^{-/-}$ MEFs. ***C***, ***D***, BrdU incorporation assay (1 h exposure) reveals that GSE can restore *Bmi1* $^{-/-}$ MEFs proliferation rate close to that of WT-GFP or WT-GSE MEFs. Results are mean ± SD of triplicates (data are representative of 4 independent cell cultures; $^{**}p < 0.01$).

were treated with 1 μM camptothecin and analyzed in a time course (Cregan et al., 2004). Our data revealed that at 24 h, ~45% of *Bmi1* $^{-/-}$ neurons had disappeared from the cultures, compared with only ~12% for WT neurons (Fig. 6). A similar trend was found at 48 h (Fig. 6). Immunostaining of the cells 24 h after treatment using an antibody against the activated form of caspase-3 revealed a marked increase in apoptotic neurons in *Bmi1* $^{-/-}$ samples compared with WT (Fig. 6*A*). To test the role of p53 in this context, we infected neurons with an adenovirus expressing a dominant-negative form of p53 (DNp53), which blocks p53 tetramerization and DNA binding-dependent transcriptional activity (Ferbeyre et al., 2002). In both WT and *Bmi1* $^{-/-}$ neurons, DNp53 rescued camptothecin-induced apoptosis (Fig. 6*A*), showing that *Bmi1* deficiency results in a p53-dependent increased sensitivity to DNA damages cause by topoisomerase I inhibition.

Exogenously added H_2O_2 induces neuronal death mainly by activation of the MST/FOXO signaling pathway (Lehtinen et al., 2006). To test the resistance of *Bmi1* $^{-/-}$ neurons to this oxidant, we treated neurons with 5 μM H_2O_2. Sixteen hours later, we analyzed cell number, caspase-3 activation, and cellular morphology. Differences in cell viability were not found between WT and *Bmi1* $^{-/-}$ neurons (Fig. 6*B*). Furthermore, addition of the DNp53 virus did not rescue either WT or *Bmi1* $^{-/-}$ neurons' viability. These data revealed that *Bmi1* deficiency does not alter neurons' sensitivity to H_2O_2.

Bmi1 $^{-/-}$ mice display a progeroid phenotype in the CNS and age is the prime risk factor to develop Alzheimer's disease. Based on this, we hypothesized that *Bmi1* $^{-/-}$ neurons are more sensitive to β-amyloid toxicity. Extracellular Aβ_{42} peptide accumulates in senile plaques of Alzheimer's patient brains, but evidence reveals that intracellular Aβ_{42} also accumulates in neurons, and that Aβ_{42}-induced cell death in neurons is mediated by p53 (Zhang et al., 2002; Ohyagi et al., 2005; LaFerla et al., 2007). We electroporated WT and *Bmi1* $^{-/-}$ neurons with plasmids driving expression of Aβ_{42}/GFP or of a mutated form lacking the first ATG. Time course analyses of cell survival at 48, 72, and 96 h after electroporation revealed that *Bmi1* $^{-/-}$ neurons were significantly more sensitive to intracellular Aβ_{42} peptide toxicity than WT neurons (Fig. 6*C*).

Bmi1 $^{-/-}$ neurons are hypersensitive to a mitochondrial toxin

Mitochondria are the main source of intracellular ROS. To test whether *Bmi1* $^{-/-}$ neurons were more sensitive to these metabo-

lites, we treated neurons with 3-nitropropionic acid (3-NP), a succinate dehydrogenase inhibitor. 3-NP exposure blocks complex II of the mitochondria respiratory chain, generates mitochondrial ROS, and leads to phase II antioxidant response genes activation by Nrf2 (Calkins et al., 2005; Shih et al., 2005). 3-NP treatment induced caspase-3-dependent (apoptosis) and caspase-3-independent (vacuolization) neuronal cell death (Fig. 7*A*). *Bmi1*$^{-/-}$ neurons were significantly more sensitive than WT neurons to both forms of 3-NP-induced cell death (Fig. 7*A*,*B*). DNp53 rescued WT and *Bmi1*$^{-/-}$ neurons from caspase-3-dependent cell death, but only rescued *Bmi1*$^{-/-}$ neurons from caspase-3-independent cell death (Fig. 7*B*). These results suggest that *Bmi1*-deficiency possibly affects neurons' capacity to scavenge mitochondrial ROS.

Identification of new *Bmi1*-regulated molecular pathways in neurons

To identify *Bmi1*-regulated molecular pathways that could explain the increase sensitivity of *Bmi1*$^{-/-}$ neurons to a mitochondrial toxin, we performed DNA microanalyses on cultured embryonic cortical neurons. Because Bmi1 is a transcriptional repressor, we first focused on upregulated genes. Our data reveal that in *Bmi1*$^{-/-}$ neurons, there is an upregulation of most previously identified Bmi1-target genes, including p16^{Ink4a}, p21^{Cip1}, and Hox genes (Hoxa5, Hoxd8, and Hoxa7), as well as previously uncharacterized Bmi1-regulated homeobox genes (Engrailed 1 and Tal1) (Table 1) (Molofsky et al., 2003). New potential Bmi1-regulated genes involved in neurogenesis (dendrin, decorin, and neuritin), cell survival (Eda2r, Gria3, and α-synuclein), or neuronal functions (AMPA3, $GABA_A$, and neurotensin) were also identified. Notably, we identified four genes involved in antioxidant defenses that are downregulated in *Bmi1*$^{-/-}$ neurons (Nrf1, GST-1α, Aldh6a1, and Sestrin1), suggesting that the oxidative metabolism may be affected by *Bmi1* deficiency (Table 1).

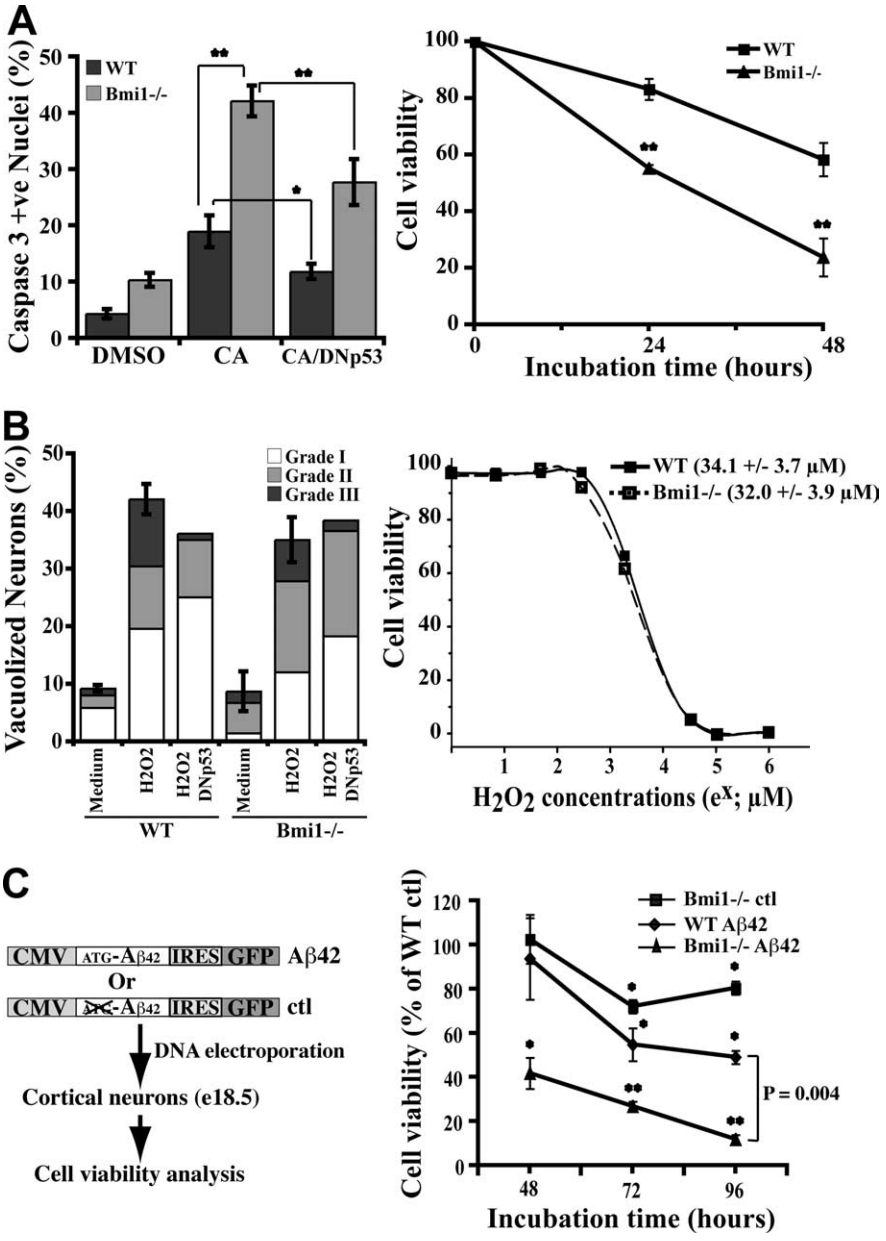

Figure 6. *Bmi1*$^{-/-}$ neurons are hypersensitive to neurotoxic agents. ***A***, Neurons were treated with camptothecin (CA; 1 μM) and labeled with MAP2 and caspase-3 antibodies. Data are expressed as the percentage of MAP2$^+$/caspase-3$^+$ cells over total MAP2$^+$ cells. Results are mean $\pm$ SD ($n = 5$; $^*p < 0.05$; $^{**}p < 0.01$) (left panel). Total number of viable neurons was calculated at time 0, 24, and 48 h after CA exposure for WT and *Bmi1*$^{-/-}$ neurons to generate a time course plot. Results are mean $\pm$ SD ($n = 3$; $^{**}p < 0.01$ compared with WT) (right panel). ***B***, Neurons were treated with H_2O_2 (5 μM), and cell death was analyzed and expressed as the percentage of vacuolized MAP2$^+$ cells over total MAP2$^+$ cells. Results are mean $\pm$ SD ($n = 5$). Vacuolization grades reflect the degree at which neurons are affected; grade I, mildly affected; grade II, moderately affected; grade III, severely affected (left panel). Total number of viable WT and *Bmi1*$^{-/-}$ neurons was calculated at various H_2O_2 concentrations to define the EC_{50} values. Data were calculated using three independent cell cultures. Values in brackets are the EC_{50} values (right panel). ***C***, Neurons were electroporated with plasmids driving expression of $A\beta_{42}$, or $A\beta_{42}$ lacking the first ATG (control). Both $A\beta_{42}$ and control constructs carried the GFP transgene. We performed the analysis by counting the total number of neurons double positive for MAP2$^+$ and GFP$^+$ staining at different time points. Data are expressed as percentages relative to control-plasmid transfected WT neurons. Results are mean $\pm$ SD ($n = 3$; $^*p < 0.05$; $^{**}p < 0.01$).

Reduced antioxidant defenses in *Bmi1*$^{-/-}$ neurons is linked to p53 activity

To test the possibility that *Bmi1* regulates the oxidative metabolism in neurons, we quantified ROS levels. Notably, we found a twofold increase in ROS concentrations in cultured *Bmi1*$^{-/-}$ neurons compared with WT (Fig. 8*A*). Infection with the DNp53 adenovirus (or supplementation with the antioxidant *N*-acetyl-cysteine) efficiently restored ROS concentrations to WT levels, suggesting that ROS accumulation in *Bmi1*$^{-/-}$ neurons is dependent on increased p53 activity (Fig. 8*A*). Because DNp53 might also interfere with the function of other proteins, including the p53-family members p63 and p73 (Jacobs et al., 2006), we further assess the specific role of p53 in this context by using *p53* knock-out mice. WT, *Bmi1*$^{-/-}$, *p53*$^{-/-}$, and *Bmi1*$^{-/-}$/*p53*$^{-/-}$ embryos were used to establish cortical neuron cultures. After 1 week, we quantified ROS levels and found that genetic ablation of *p53* could also prevent ROS

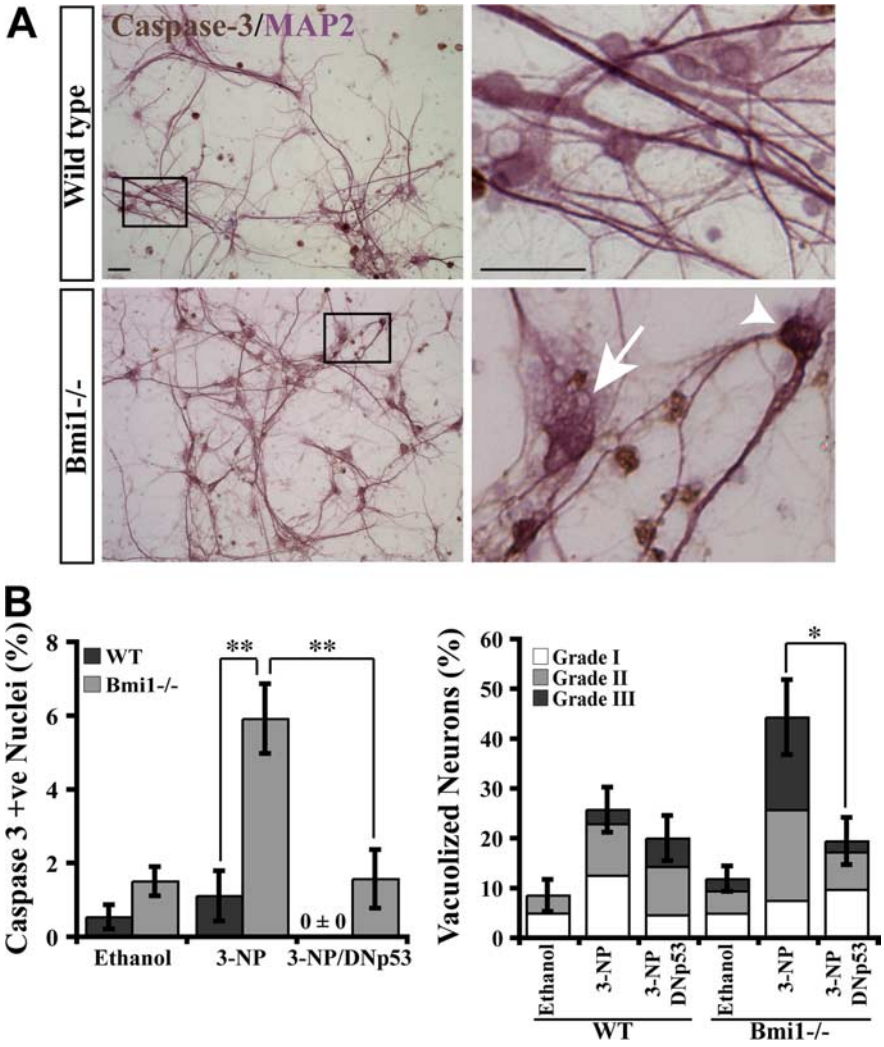

Figure 7. *Bmi1* $^{-/-}$ neurons are hypersensitive to the mitochondrial toxin 3-NP. ***A***, ***B***, E18.5 WT and *Bmi1* $^{-/-}$ neurons were exposed to 3-NP (2 mM) for 16 h. ***A***, Neurons were labeled with caspase-3 (brown) and MAP2 (pink) antibodies, and analyzed by IHC. Upon 3-NP exposure, most *Bmi1* $^{-/-}$ neurons presented caspase-3-dependent (arrowhead) or caspase-3-independent (vacuolization; arrow) cell death. Caspase-3-positive nuclei not expressing MAP2 represent remains of dead astrocytes or fibroblasts. Scale bar, 20 μm. ***B***, Data are expressed as the percentage of MAP2 $^{+}$/caspase-3 $^{+}$ cells over total MAP2 $^{+}$ cells (left panel) or as the percentage of vacuolized MAP2 $^{+}$ cells over total MAP2 $^{+}$ cells (right panel). Vacuolization grades are as described in Figure 6*B*. Results are mean ± SD ($n = 5$; *$p < 0.05$; **$p < 0.01$).

accumulation in *Bmi1* $^{-/-}$ neurons (Fig. 8*B*). These results suggest that in *Bmi1* $^{-/-}$ neurons, p53 is stabilized or activated, resulting in elevated ROS concentrations.

To address how *Bmi1* deficiency leads to elevated ROS concentrations, we evaluated the expression of several antioxidant genes, including those previously linked to *p53* activity, i.e., GSTα1, NQO1, xCT, Sestrin1, Sestrin2, Cu/Zn superoxide dismutase (Sod1), and Mn superoxide dismutase (Sod2) in WT, *Bmi1* $^{-/-}$, *Bmi1* $^{-/-}$/*p53* $^{-/-}$, or DNp53-infected *Bmi1* $^{-/-}$ cultured neurons (Sablina et al., 2005; Dhar et al., 2006; Faraonio et al., 2006; Matheu et al., 2007). We found that compared with WT, expression of all tested genes was reduced in *Bmi1* $^{-/-}$ neurons, and that this reduction was most dramatic for phase II genes (Fig. 8*C*). Importantly, DNp53 could restore the expression of most genes to WT levels in *Bmi1* $^{-/-}$ neurons, similarly as genetic ablation of *p53* (Fig. 8*C*,*D*). We also cultured neurons at 3% oxygen concentration. We found that reducing oxygen concentration had no impact on ROS levels in *Bmi1* $^{-/-}$ and *Bmi1* $^{-/-}$/*p53* $^{-/-}$ neurons (Fig. 9*A*, data not shown). These results reveal that abnormal antioxidant gene expression in *Bmi1* $^{-/-}$ neurons is genetically linked to *p53* activity.

To further explore the underlying molecular mechanism, we compared the expression of Sirt1, peroxisome proliferator-activated receptor gamma coactivator-1 α (PGC-1α), and Nrf2 in WT and *Bmi1* $^{-/-}$ neurons. PGC-1α and Nrf2 are activators of antioxidant defense genes in neurons, and Sirt1 can promote PGC-1α activity by deacetylation (Calkins et al., 2005; Shih et al., 2005; St-Pierre et al., 2006; Kim et al., 2007). Sirt1, PGC-1α, and Nrf2 protein levels were modestly increased in *Bmi1* $^{-/-}$ neurons, and the acetylated form of PGC-1α was slightly reduced (Fig. 8*E*). No significant variations in gene expression were found by quantitative RT-PCR (data not shown). Thus, expression levels of PGC-1α, Nrf2, and Sirt1 are close to normal in *Bmi1* $^{-/-}$ neurons.

To test the possibility that antioxidant genes are actively repressed by p53 in *Bmi1* $^{-/-}$ neurons, we performed ChIP experiments at the *xCT* and *Sod2* promoters. When compared with WT, we found that p53 was enriched at the *xCT* and *Sod2* promoters in *Bmi1* $^{-/-}$ neurons, and this correlated with a repressed chromatin state, as shown by the accumulation of bimethylated histone H3 at lysine 9 and 27 (Fig. 8*F*) (Sparmann and van Lohuizen, 2006). No variations were found for acetylated histone H4, a mark of active chromatin. We also assess whether p53 accumulation at these regions of the chromatin was accompanied by the presence of corepressors. HDAC3/N-CoR and HDAC1/Sin3a corepressor complexes have been described in various systems (Jepsen and Rosenfeld, 2002; Karagianni and Wong, 2007). We found that HDAC1 and N-CoR were enriched at the *xCT* and *Sod2* promoters in *Bmi1* $^{-/-}$ neurons. No variations were found at the *β-globin* promoter, which was used as an internal control (Fig. 8*F*). These findings suggest that *Bmi1* deficiency results in increased ROS concentration in neurons due to a repressive action of p53 on the expression of antioxidant genes (see model in Fig. 9*C*).

P53 is pro-oxidant in neurons and in the CNS in physiological conditions

In physiological conditions, *p53* is proposed to have an antioxidant activity in most tissue and primary cell lines, such as in embryonic lung fibroblasts (Matheu et al., 2007). However, we found that genetic ablation of *p53* in *Bmi1* $^{-/-}$ neurons could restore ROS to normal levels, showing that *p53* is pro-oxidant in this pathological context. To explore the possibility that *p53* is also pro-oxidant in neurons in physiological conditions, we established neuronal and lung fibroblast cultures from WT and *p53* $^{-/-}$ embryos at 3% and 20% oxygen concentration. At day 7 after plating (neurons) or passage 1 (lung fibroblasts), we mea-

Table 1. List of genes whose expression is modulated in cultured *Bmi1*$^{-/-}$ neurons

	Accession	Fold	*p* value	qPCR
Upregulated genes				
Cyclin-dependent kinase inhibitor 2A (Cdkn2a), mRNA	NM_001040654	5.43	0.0012	85.5 ± 12.0
Decorin (Dcn), mRNA	NM_007833	3.92	0.0170	1.8 ± 0.1
Cyclin-dependent kinase inhibitor 1A (P21) (Cdkn1a), mRNA	NM_001111099	3.48	0.0011	1.5 ± 0.1
Homeobox A5 (Hoxa5), mRNA	NM_001111099	3.35	0.0068	nd
Neurotensin (Nts), mRNA	NM_024435	3.27	0.0245	nd
Engrailed 1 (En1), mRNA	NM_010133	3.13	0.0044	nd
Dendrin (Ddn), mRNA	NM_001013741	3.07	0.0370	1.9 ± 0.1
Homeobox D8 (Hoxd8), mRNA	NM_008276	2.87	0.0031	nd
T-cell acute lymphocytic leukemia 1 (Tal1), mRNA	NM_011527	2.83	0.0001	nd
Ectodysplasin receptor (Eda2r), mRNA	NM_175540	2.52	0.0343	4.1 ± 0.6
Homeobox A7 (Hoxa7), mRNA	NM_010455	2.42	0.0089	194.3 ± 31.1
Heparan sulfate D-glucosamyl 3-*O*-sulfotransferase-2 (HS3ST2), mRNA	NM_001081327	2.36	0.0415	nd
Potassium voltage-gated channel, Shaw-related subfamily, member 4 (Kcnc4), mRNA	NM_145922	2.33	0.0012	nd
Crystallin, mu (Crym), mRNA	NM_016669	2.31	0.0004	nd
Regulator of G-protein signaling 4 (Rgs4), mRNA	NM_009062	2.31	0.0175	nd
Guanine deaminase (Gda), mRNA	NM_010266	2.30	0.0313	nd
Neuritin 1 (Nrn1), mRNA	NM_153529	2.30	0.0010	nd
Fos-like antigen 2 (Fosl2), mRNA	NM_008037	2.30	0.0035	nd
Glutamate receptor, ionotropic, AMPA3 (α3) (Gria3), mRNA	NM_016886	2.29	0.0010	nd
Synuclein, α (Snca), mRNA	NM_009221	2.26	0.0183	1.9 ± 0.2
RAS protein-specific guanine nucleotide-releasing factor 1 (Rasgrf1), mRNA	NM_011245	2.25	0.0057	nd
Epoxide hydrolase 1, microsomal (Ephx1), mRNA	NM_010145	2.21	0.0205	nd
Growth differentiation factor 10 (Gdf10), mRNA	NM_145741	2.17	0.0119	nd
Argininosuccinate synthetase 1 (Ass1), mRNA	NM_007494	2.12	0.0032	nd
$GABA_A$ receptor, subunit β 1 (Gabrb1), mRNA	NM_008069	2.09	0.0097	nd
Cyclin-dependent kinase inhibitor 2B (p15, inhibits CDK4) (Cdkn2b), mRNA	NM_007670	2.07	0.0014	nd
Contactin-associated protein 4 (Cntnap4), mRNA	NM_130457	2.04	0.0148	nd
Insulin-like growth factor 2 (Igf2), mRNA	NM_001122737	2.02	0.0010	nd
Glycine receptor, α2 subunit (Glra2), mRNA	NM_183427	2.02	0.0162	nd
Downregulated genes				
Nuclear respiratory factor 1 (Nrf1), mRNA	NM_010938	0.82	0.0245	0.5 ± 0.1
Similar to glutathione *S*-transferase, mRNA	XM_001473911	0.80	0.0411	0.3 ± 0.1
Sestrin 1 (Sesn1), mRNA	NM_001013370	0.72	0.0014	0.6 ± 0.1
Aldehyde dehydrogenase family 6, subfamily A1 (Aldh6a1), mRNA	NM_134042	0.72	0.0389	nd

nd, Not determined.

sured ROS level and compared gene expression. Notably, *p53*$^{-/-}$ neurons showed reduced ROS level when compared with WT at both oxygen concentrations (Fig. 9*A*). In contrast, *p53*$^{-/-}$ lung fibroblasts presented increased ROS concentrations in the same conditions (Fig. 9*B*). Consistently, *p53* deficiency in neurons resulted in upregulation of *xCT*, *GSTα1*, *NQO1*, and *Sestrin1* expression when compared with WT, with the exception of *Sestrin2*, which expression was modestly reduced (Fig. 9*A*). In contrast, *GSTα1*, *NQO1*, and *Sestrin2* expression was reduced in *p53*$^{-/-}$ lung fibroblasts, while *Sestrin1* expression was increased (Fig. 9*B*). Little variations in ROS levels were observed by modifying oxygen concentration in neurons, but not in MELFs (Fig. 9*A*,*B*). To validate these observations *in vivo*, we compared lipid peroxidation and gene expression in the brain, lung, and liver of WT and *p53*$^{-/-}$ littermates at 2 months of age. Lipid peroxidation is the result of cumulative oxidative damage to cell membranes and thus reflects imbalance in ROS levels. Analysis of older *p53*-null mice was not possible due to the rapid development of tumors in these animals. When compared with WT, we found that lipid peroxidation levels were much higher in the liver and lung of *p53*$^{-/-}$ mice and significantly lower (by 42%) in the brain (Table 2). Furthermore, real-time PCR analyses revealed that antioxidant gene expression levels are significantly higher in the cortex of *p53*-null mice than in their WT littermates (Table 2). Thus, in sharp contrast with the proposed general antioxidant function of *p53* (Matheu et al., 2007), our results demonstrate that *p53* is pro-oxidant in neurons and in the CNS of mammals in pathological and physiological conditions (see model in Fig. 9*C*).

Discussion

The Bmi1 oncogene has been extensively studied for its role in the maintenance of cell proliferation (Sparmann and van Lohuizen, 2006). However, Bmi1 is also widely expressed in postmitotic ocular tissues and in neurons of the adult CNS (this study). Here, we uncover a new function for *Bmi1* in controlling survival and antioxidant defenses in neurons through repression of *p53* pro-apoptotic and pro-oxidant activities. These findings have implications for the understanding of normal CNS aging and age-related neurodegenerative diseases.

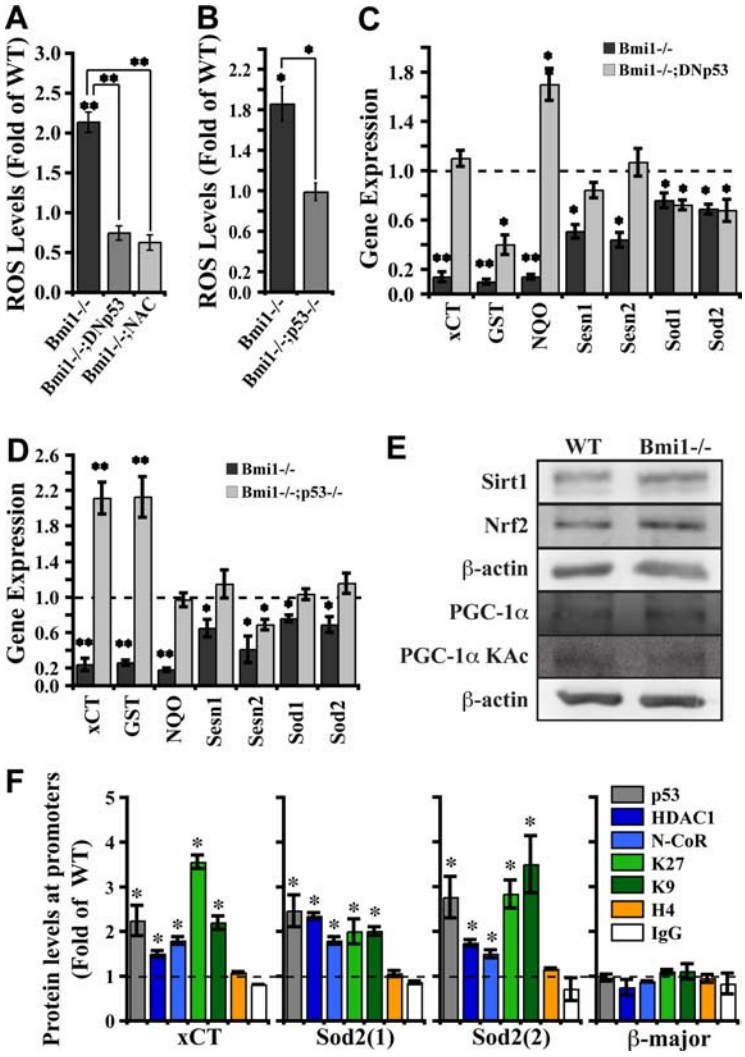

Figure 8. Antioxidant defenses are deficient in *Bmi1*$^{-/-}$ neurons. ***A***, ROS concentrations were measured with the fluorescent dye DCFDA. Data were normalized to the protein contents and expressed as fold change relative to WT. Results are mean ± SD ($n = 3$ independent cultures; *$p < 0.05$; **$p < 0.01$). ***B***, ROS levels in *Bmi1*$^{-/-}$ and *Bmi1*$^{-/-}$/*p53*$^{-/-}$ neurons. Measurements were done as in ***A***. ***C***, ***D***, Gene expression levels were analyzed by real-time PCR in *Bmi1*$^{-/-}$, DNp53-infected *Bmi1*$^{-/-}$, and *Bmi1*$^{-/-}$/*p53*$^{-/-}$ neurons. Dashed lines represent the basal gene expression level measured in WT neurons (normalized to 1). Results are mean ± SD ($n = 5$ independent cultures; *$p < 0.05$; **$p < 0.01$). ***E***, Western blot analysis of neuronal extracts for the expression of Sirt1, Nrf2, and total and acetylated forms of PGC-1α. For PGC-1α detection, proteins were immunoprecipitated with an anti-PGC-1α antibody and Western blotting were done using anti-PGC-1α antibody (total PGC-1α), or an anti-acetylated-lysine (K acet.). β-Actin was used as loading reference. ***F***, Chromatin immunoprecipitation was performed with WT and *Bmi1*$^{-/-}$ neuronal extracts. Immunoprecipitated DNA/protein complexes were analyzed using primers directed against the *xCT*, *Sod2* (2 sites), and *β-major* promoters. Results are mean ± SD ($n = 3$ independent cultures; *$p < 0.05$ compared with values in WT set at 1).

Bmi1 and the p19^{Arf}/p53 pathway

We have shown that *in vivo*, *p19*^{Arf} RNA and protein expression levels are increased in *Bmi1*$^{-/-}$ neurons, and that the downstream p53 apoptotic cascade is activated. *In vitro*, *Bmi1*$^{-/-}$ neurons have increased total and activated p53 protein levels, are hypersensitive to camptothecin-induced apoptosis, and can be rescued by the DNp53 virus. These data suggest that p53 mediates most of the apoptotic phenotype observed in *Bmi1*$^{-/-}$ neurons. We also found that *Bmi1*$^{-/-}$ neurons also present abnormally high free radical concentrations and are hypersensitive to a mitochondrial toxin, implying a role for *Bmi1* in regulation of mitochondria oxidative metabolism. Genetic inactivation of *p53* revealed that deregulation of the oxidative metabolism in *Bmi1*$^{-/-}$ neurons is mostly, if not entirely, mediated by *p53*. This is supported by the observation that antioxidant gene levels in *Bmi1*$^{-/-}$/*p53*$^{-/-}$ neurons (where xCT and GST have supraphysiologic levels) are almost identical to those observed in *p53*$^{-/-}$ neurons (compare Fig. 8*D* with Fig. 9*A*). However, total ROS levels are apparently distinct between *Bmi1*$^{-/-}$/*p53*$^{-/-}$ and *p53*$^{-/-}$ neurons (compare Fig. 8*B* with Fig. 9*A*). These observations suggest that most but maybe not all *Bmi1* functions are mediated through repression of *p53* activity. These additional functions may be explained by p19^{Arf}-mediated actions through Mdm2 on the p63 and p73 protein variants, which are also expressed in CNS neurons (Jacobs et al., 2006).

P53 and CNS aging

Upon accumulation of mutations, p53 promotes apoptosis or senescence in premalignant tissues to prevent carcinogenesis (Sherr, 2001; Sharpless et al., 2004). One way p53 may promote mitochondria-mediated cell death in dividing cells is by increasing ROS concentrations through repression of antioxidant genes (Dhar et al., 2006; Faraonio et al., 2006). Paradoxically, p53 was proposed to stimulate antioxidant defenses in various organs in physiological conditions through its positive action on Sestrin(s), and thus protect the genome from accumulation of mutations by lowering intracellular ROS levels (Sablina et al., 2005; Matheu et al., 2007). During development, *p53* has a function in eliminating supernumerary neurons and neuronal progenitors (Jacobs et al., 2006). Later on, *p53* is required to prevent tumor development from progenitor/stem cells, oligodendrocytes, or astrocytes. However, p53 activity is apparently not required in adult neurons, which are postmitotic and not tumor prone. Rather, all evidence suggests that p53 activity in neurons is pathological (Zhang et al., 2002; Bae et al., 2005; Ohyagi et al., 2005; Nair, 2006; Nair et al., 2006; Kieran et al., 2007).

We found here that in contrast with other organs and cultured lung fibroblasts, *p53* is pro-oxidant in brain tissue and cultured neurons. Our data argue that *p53* is always active in neurons to levels that are pro-oxidant, in sharp contrast with other cell types. Notably, expression of a dominant-negative form of p53 in the CNS of *Drosophila*, but not in other organs, was shown to result in lifespan extension and improved resistance to paraquat, suggesting that the deleterious function of p53 in neurons is conserved in insects (Bauer et al., 2005). These observations may explain why transgenic mice with extra copies of *p53* and *p19*^{Arf} do not have an increase in maximum lifespan, despite being protected from tumor burden (Matheu et al., 2007). In these animals, increasing p53 gene dosage is predicted to increase oxidative damage accumulation in the CNS, which is unlikely to promote lifespan extension.

Bmi1, aging, and neurodegenerative diseases

The function of *Bmi1* on the antioxidant defense system appears to overlap only partially with that of *PGC-1α*. *PGC-1α*$^{-/-}$ mice show only a modest reduction in the basal expression level of Sod1, Sod2, and catalase genes in the brain, but *PGC-1α*$^{-/-}$ cells are highly inefficient to activate antioxidant genes expression when challenged with oxidants (St-Pierre et al., 2006). In contrast, *Bmi1*$^{-/-}$ neurons have abnormally low basal expression levels for most antioxidant genes, yet can still respond to 3-NP treatment by activating phase II gene expression, although less efficiently (data not shown). These observations suggest that *Bmi1* deficiency results in the constitutive repression of antioxidant genes (model in Fig. 9), while *PGC-1α* deficiency results in defective activation of antioxidant genes upon acute oxidative stress. In contrast to *Bmi1*$^{-/-}$ neurons, *PGC-1α*$^{-/-}$ cells are also more sensitive to the action of H_2O_2. Importantly, catalase, which scavenges H_2O_2, is mostly present in the nonmitochondrial cytoplasm and peroxisomes, and thus may be more protective against exogenous H_2O_2 than against mitochondrial ROS. Catalase is the only antioxidant gene we tested which expression is unaffected in *Bmi1*$^{-/-}$ neurons.

The free radical theory of aging proposes that cellular and DNA damage produced by mitochondrial ROS are the causal factor of cellular and organismal aging (Harman, 1956), and we have shown here that loss of *Bmi1* leads to a dramatic reduction in antioxidant defenses and to concomitant increase in ROS concentrations. Furthermore, *Bmi1*$^{-/-}$ neurons are hypersensitive to neurotoxic agents and have an elevated level of spontaneous apoptosis in nontoxic conditions when compared with WT neurons. Together, these results provide a most plausible mechanism to explain why *Bmi1*-deficient mice and neurons age prematurely. In the context of normal aging, our finding brings the possibility that reduced *BMI1* expression in human brain neurons may contribute to the age-associated reduction in antioxidant defenses, leading to accumulation of oxidative damage and to neuronal dysfunction. The activity of *Bmi1* against mitochondrial ROS may be also relevant to age-associated neurodegenerative diseases where cell death is apparently mediated by oxidative damage, such as in Parkinson disease (Thomas and Beal, 2007). *Bmi1* activity against p53-mediated neuronal apoptosis may be relevant to Alzheimer's and Huntington's diseases. P53 expression is increased in Alzheimer's disease brains, its transcription is activated by intracellular $A\beta_{42}$, and p53 inhibition prevents $A\beta_{42}$-induced neuronal cell death (Zhang et al., 2002; Ohyagi et al., 2005). We found here that *Bmi1* deficiency sensitizes neurons to apoptosis induced by the intracellular $A\beta_{42}$ peptide. Because this system is far from physiological conditions, more work will be required to evaluate the possible implication of BMI1 in Alzheimer's disease. In the Huntington's disease brain, complex II activity is reduced, and 3-NP administration results in a striatal movement disorder in rodents and primates resembling Huntington's disease (Lin and Beal, 2006). Notably, p53 is activated by mutant Huntingtin protein (Bae et al., 2005). We found that *Bmi1* deficiency dramatically increases neurons' vulnerability to 3-NP toxicity and that p53 inhibition can rescue this phenotype. Our study reveals how the activity of *Bmi1* in postmitotic neurons is required to block the induction of a proapoptotic and pro-oxidant molecular aging program mostly driven by *p53*.

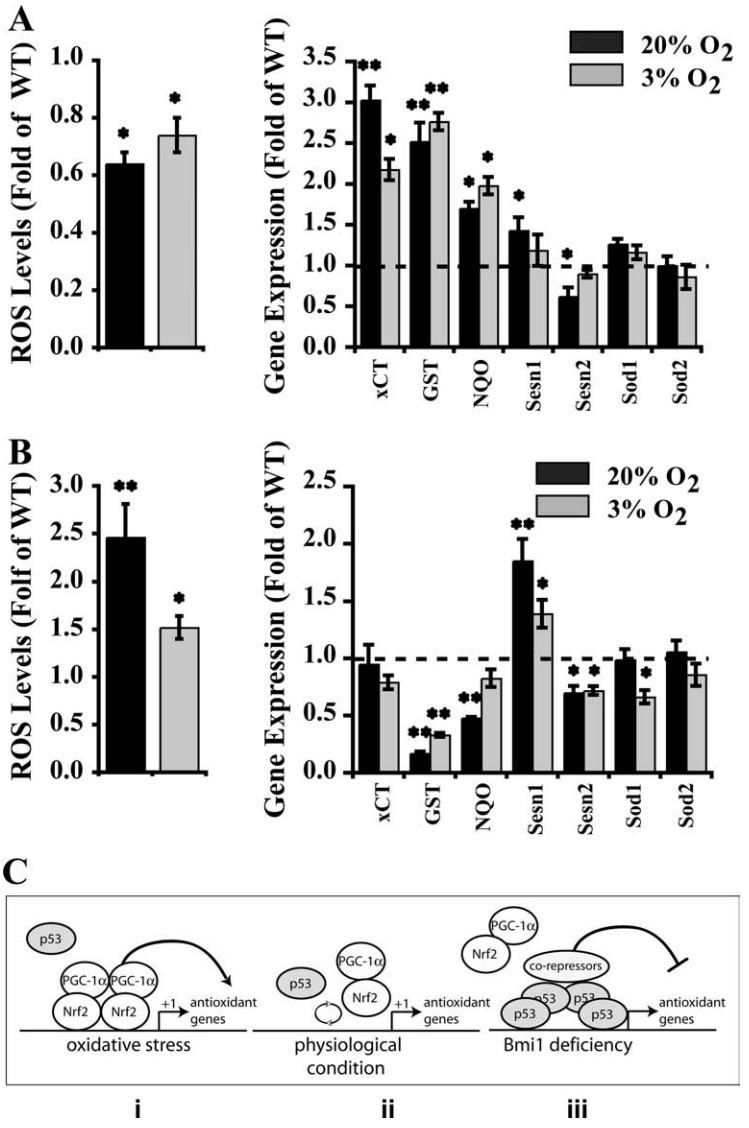

Figure 9. *p53* is pro-oxidant in cultured neurons and in the CNS. ***A***, ROS levels in WT and *p53*$^{-/-}$ neurons cultured at 3% or 20% oxygen concentrations. Data are represented as fold change relative to WT samples. Results are mean ± SD ($n = 3$; $^*p < 0.05$) (left panel). Expression levels of antioxidant genes in *p53*$^{-/-}$ neurons were analyzed by real-time PCR. Dashed line represents the basal gene expression level measured in WT neurons (normalized to 1). Results are mean ± SD ($n = 3$ independent cultures; $^*p < 0.05$; $^{**}p < 0.01$) (right panel). ***B***, ROS (left panel) and gene expression (right panel) levels in WT and *p53*$^{-/-}$ mouse embryonic lung fibroblasts (MELFs) were analyzed as in (***A***) ($n = 3$; $^*p < 0.05$; $^{**}p < 0.01$). ***C***, Working model. ***i***, Upon oxidative stress, Nrf2 and PGC-1α are recruited to antioxidant gene promoters to induce transcription. ***ii***, In physiological condition, p53 may compete or not with Nrf2 and PGC-1α for association at promoters, establishing equilibrium. ***iii***, *Bmi1* deficiency leads to increase p53 accumulation at promoters and to gene repression through recruitment of corepressors. The p53 repressor complex may or may not displace Nrf2 and PGC-1α from the promoter.

Table 2. *P53* is pro-oxidant in the central nervous system

	Tissues		
	Liver	Lung	Cortex
MDA adduct[a]	1.58 ± 0.13*	1.91 ± 0.11*	0.58 ± 0.04*
Gene expression levels[b]			
xCT	0.24 ± 0.01*	0.35 ± 0.04*	1.65 ± 0.11*
GST	1.70 ± 0.19*	0.78 ± 0.09*	1.78 ± 0.03*
NQO	0.94 ± 0.03	0.43 ± 0.08*	1.37 ± 0.07*
Sesn1	0.85 ± 0.03*	0.31 ± 0.06*	1.53 ± 0.17*
Sesn2	0.24 ± 0.01*	0.27 ± 0.04*	1.48 ± 0.04*
Sod1	0.90 ± 0.03	0.87 ± 0.03*	1.42 ± 0.04*
Sod2	0.78 ± 0.03*	0.61 ± 0.03*	1.00 ± 0.09

[a]Lipid peroxidation was measured in p53$^{-/-}$ liver, lung, and brain homogenates as concentration of MDA. Data were normalized to sample protein contents and are represented as fold change relative to WT samples set at 1. Results are mean ± SD ($n = 3–5$; $*p < 0.05$).

[b]Real-time PCR analysis of antioxidant gene expression levels in p53$^{-/-}$ liver, lung, and brain. Data are represented as fold change relative to WT samples set at 1. Results are mean ± SD ($n = 3–4$; $*p < 0.05$).

References

Bae BI, Xu H, Igarashi S, Fujimuro M, Agrawal N, Taya Y, Hayward SD, Moran TH, Montell C, Ross CA, Snyder SH, Sawa A (2005) p53 mediates cellular dysfunction and behavioral abnormalities in Huntington's disease. Neuron 47:29–41.

Balaban RS, Nemoto S, Finkel T (2005) Mitochondria, oxidants, and aging. Cell 120:483–495.

Bauer JH, Poon PC, Glatt-Deeley H, Abrams JM, Helfand SL (2005) Neuronal expression of p53 dominant-negative proteins in adult *Drosophila melanogaster* extends life span. Curr Biol 15:2063–2068.

Beauséjour CM, Krtolica A, Galimi F, Narita M, Lowe SW, Yaswen P, Campisi J (2003) Reversal of human cellular senescence: roles of the p53 and p16 pathways. EMBO J 22:4212–4222.

Buege JA, Aust SD (1978) Microsomal lipid peroxidation. Methods Enzymol 52:302–310.

Calkins MJ, Jakel RJ, Johnson DA, Chan K, Kan YW, Johnson JA (2005) Protection from mitochondrial complex II inhibition in vitro and in vivo by Nrf2-mediated transcription. Proc Natl Acad Sci U S A 102:244–249.

Cregan SP, Arbour NA, Maclaurin JG, Callaghan SM, Fortin A, Cheung EC, Guberman DS, Park DS, Slack RS (2004) p53 activation domain 1 is essential for PUMA upregulation and p53-mediated neuronal cell death. J Neurosci 24:10003–10012.

Dhar SK, Xu Y, Chen Y, St Clair DK (2006) Specificity protein 1-dependent p53-mediated suppression of human manganese superoxide dismutase gene expression. J Biol Chem 281:21698–21709.

Dimri GP, Lee X, Basile G, Acosta M, Scott G, Roskelley C, Medrano EE, Linskens M, Rubelj I, Pereira-Smith O, et al (1995) A biomarker that identifies senescent human cells in culture and in aging skin in vivo. Proc Natl Acad Sci U S A 92:9363–9367.

Faraonio R, Vergara P, Di Marzo D, Pierantoni MG, Napolitano M, Russo T, Cimino F (2006) p53 suppresses the Nrf2-dependent transcription of antioxidant response genes. J Biol Chem 281:39776–39784.

Ferbeyre G, de Stanchina E, Lin AW, Querido E, McCurrach ME, Hannon GJ, Lowe SW (2002) Oncogenic ras and p53 cooperate to induce cellular senescence. Mol Cell Biol 22:3497–3508.

Fortin A, Cregan SP, MacLaurin JG, Kushwaha N, Hickman ES, Thompson CS, Hakim A, Albert PR, Cecconi F, Helin K, Park DS, Slack RS (2001) APAF1 is a key transcriptional target for p53 in the regulation of neuronal cell death. J Cell Biol 155:207–216.

Halliwell B (2006) Oxidative stress and neurodegeneration: where are we now? J Neurochem 97:1634–1658.

Harman D (1956) Aging: a theory based on free radical and radiation chemistry. J Gerontol 11:298–300.

Ihanamäki T, Salminen H, Säämänen AM, Pelliniemi LJ, Hartmann DJ, Sandberg-Lall M, Vuorio E (2001) Age-dependent changes in the expression of matrix components in the mouse eye. Exp Eye Res 72:423–431.

Jacobs JJ, Kieboom K, Marino S, DePinho RA, van Lohuizen M (1999) The oncogene and Polycomb-group gene bmi-1 regulates cell proliferation and senescence through the ink4a locus. Nature 397:164–168.

Jacobs WB, Kaplan DR, Miller FD (2006) The p53 family in nervous system development and disease. J Neurochem 97:1571–1584.

Jepsen K, Rosenfeld MG (2002) Biological roles and mechanistic actions of co-repressor complexes. J Cell Sci 115:689–698.

Karagianni P, Wong J (2007) HDAC3: taking the SMRT-N-CoRrect road to repression. Oncogene 26:5439–5449.

Kieran D, Woods I, Villunger A, Strasser A, Prehn JH (2007) Deletion of the BH3-only protein puma protects motoneurons from ER stress-induced apoptosis and delays motoneuron loss in ALS mice. Proc Natl Acad Sci U S A 104:20606–20611.

Kim D, Nguyen MD, Dobbin MM, Fischer A, Sananbenesi F, Rodgers JT, Delalle I, Baur JA, Sui G, Armour SM, Puigserver P, Sinclair DA, Tsai LH (2007) SIRT1 deacetylase protects against neurodegeneration in models for Alzheimer's disease and amyotrophic lateral sclerosis. EMBO J 26:3169–3179.

Krishnamurthy J, Torrice C, Ramsey MR, Kovalev GI, Al-Regaiey K, Su L, Sharpless NE (2004) Ink4a/Arf expression is a biomarker of aging. J Clin Invest 114:1299–1307.

LaFerla FM, Green KN, Oddo S (2007) Intracellular amyloid-beta in Alzheimer's disease. Nat Rev Neurosci 8:499–509.

Lehtinen MK, Yuan Z, Boag PR, Yang Y, Villén J, Becker EB, DiBacco S, de la Iglesia N, Gygi S, Blackwell TK, Bonni A (2006) A conserved MST-FOXO signaling pathway mediates oxidative-stress responses and extends life span. Cell 125:987–1001.

Lessard J, Sauvageau G (2003) Bmi-1 determines the proliferative capacity of normal and leukaemic stem cells. Nature 423:255–260.

Lin MT, Beal MF (2006) Mitochondrial dysfunction and oxidative stress in neurodegenerative diseases. Nature 443:787–795.

Matheu A, Maraver A, Klatt P, Flores I, Garcia-Cao I, Borras C, Flores JM, Viña J, Blasco MA, Serrano M (2007) Delayed ageing through damage protection by the Arf/p53 pathway. Nature 448:375–379.

Molofsky AV, Pardal R, Iwashita T, Park IK, Clarke MF, Morrison SJ (2003) Bmi-1 dependence distinguishes neural stem cell self-renewal from progenitor proliferation. Nature 425:962–967.

Nair VD (2006) Activation of p53 signaling initiates apoptotic death in a cellular model of Parkinson's disease. Apoptosis 11:955–966.

Nair VD, McNaught KS, González-Maeso J, Sealfon SC, Olanow CW (2006) p53 mediates nontranscriptional cell death in dopaminergic cells in response to proteasome inhibition. J Biol Chem 281:39550–39560.

Ohyagi Y, Asahara H, Chui DH, Tsuruta Y, Sakae N, Miyoshi K, Yamada T, Kikuchi H, Taniwaki T, Murai H, Ikezoe K, Furuya H, Kawarabayashi T, Shoji M, Checler F, Iwaki T, Makifuchi T, Takeda K, Kira J, Tabira T (2005) Intracellular Abeta42 activates p53 promoter: a pathway to neurodegeneration in Alzheimer's disease. FASEB J 19:255–257.

Park IK, Qian D, Kiel M, Becker MW, Pihalja M, Weissman IL, Morrison SJ, Clarke MF (2003) Bmi-1 is required for maintenance of adult self-renewing haematopoietic stem cells. Nature 423:302–305.

Parrinello S, Samper E, Krtolica A, Goldstein J, Melov S, Campisi J (2003) Oxygen sensitivity severely limits the replicative lifespan of murine fibroblasts. Nat Cell Biol 5:741–747.

Radák Z, Chung HY, Naito H, Takahashi R, Jung KJ, Kim HJ, Goto S (2004) Age-associated increase in oxidative stress and nuclear factor kappaB activation are attenuated in rat liver by regular exercise. FASEB J 18:749–750.

Sablina AA, Budanov AV, Ilyinskaya GV, Agapova LS, Kravchenko JE, Chumakov PM (2005) The antioxidant function of the p53 tumor suppressor. Nat Med 11:1306–1313.

Sharpless NE, Ramsey MR, Balasubramanian P, Castrillon DH, DePinho RA (2004) The differential impact of p16(INK4a) or p19(ARF) deficiency on cell growth and tumorigenesis. Oncogene 23:379–385.

Sherr CJ (2001) The INK4a/ARF network in tumour suppression. Nat Rev Mol Cell Biol 2:731–737.

Sherr CJ (2006) Divorcing ARF and p53: an unsettled case. Nat Rev Cancer 6:663–673.

Shih AY, Imbeault S, Barakauskas V, Erb H, Jiang L, Li P, Murphy TH (2005) Induction of the Nrf2-driven antioxidant response confers neuroprotection during mitochondrial stress in vivo. J Biol Chem 280:22925–22936.

Silver J, Miller JH (2004) Regeneration beyond the glial scar. Nat Rev Neurosci 5:146–156.

Sparmann A, van Lohuizen M (2006) Polycomb silencers control cell fate, development and cancer. Nat Rev Cancer 6:846–856.

St-Pierre J, Drori S, Uldry M, Silvaggi JM, Rhee J, Jäger S, Handschin C, Zheng K, Lin J, Yang W, Simon DK, Bachoo R, Spiegelman BM (2006) Suppression of reactive oxygen species and neurodegeneration by the PGC-1 transcriptional coactivators. Cell 127:397–408.

Tang Y, Zhao W, Chen Y, Zhao Y, Gu W (2008) Acetylation is indispensable for p53 activation. Cell 133:612–626.

The Italian-American Cataract Study Group (1991) Risk factors for age-related cortical, nuclear, and posterior subcapsular cataracts. Am J Epidemiol 133:541–553.

Thomas B, Beal MF (2007) Parkinson's disease. Hum Mol Genet 16 Spec No 2:R183–R194.

Tyner SD, Venkatachalam S, Choi J, Jones S, Ghebranious N, Igelmann H, Lu X, Soron G, Cooper B, Brayton C, Hee Park S, Thompson T, Karsenty G, Bradley A, Donehower LA (2002) p53 mutant mice that display early ageing-associated phenotypes. Nature 415:45–53.

Valk-Lingbeek ME, Bruggeman SW, van Lohuizen M (2004) Stem cells and cancer; the polycomb connection. Cell 118:409–418.

Vaziri H, Dessain SK, Ng Eaton E, Imai SI, Frye RA, Pandita TK, Guarente L, Weinberg RA (2001) hSIR2(SIRT1) functions as an NAD-dependent p53 deacetylase. Cell 107:149–159.

Wolf N, Penn P, Pendergrass W, Van Remmen H, Bartke A, Rabinovitch P, Martin GM (2005) Age-related cataract progression in five mouse models for anti-oxidant protection or hormonal influence. Exp Eye Res 81:276–285.

Zhang Y, McLaughlin R, Goodyer C, LeBlanc A (2002) Selective cytotoxicity of intracellular amyloid beta peptide1–42 through p53 and Bax in cultured primary human neurons. J Cell Biol 156:519–529.